Atmos. Chem. Phys. Discuss., 12, 351–385, 2012
www.atmos-chem-phys-discuss.net/12/351/2012/
doi:10.5194/acpd-12-351-2012

Atmospheric Chemistry and Physics Discussions

Potential indirect effects of aerosol on tropical cyclone intensity: convective fluxes and cold-pool activity

G. M. Krall and W. R. Cottom

Department of Atmospheric Science, Colorado State University, Fort Collins, USA

Received: 25 April 2011 – Accepted: 19 September 2011 – Published: 5 January 2012

Correspondence to: W. R. Cotton (cotton@atmos.colostate.edu)

Published by Copernicus Publications on behalf of the European Geosciences Union.

Abstract

Observational and model evidence suggest that a 2008 Western Pacific typhoon (NURI) ingested elevated concentrations of aerosol as it neared the Chinese coast. This study uses a regional model with two-moment bin-emulating microphysics to simulate the typhoon as it enters the field of elevated aerosol concentrations. A clean maritime field of cloud condensation nuclei (CCN) was prescribed as marine background CCN concentrations and then based on satellite and global aerosol model output, increased to pollution levels and further enhanced in sensitivity tests. The typhoon was simulated for 96 h beginning 17 August 2008. During the final 60 h CCN concentrations were enhanced as it neared the Philippines and coastal China. The model was initialized with both global reanalysis model data and irregularly spaced dropsonde data from the 2008 T-PARC observational campaign using an objective analysis routine. At 36 h, the internal nudging of the model was switched off and allowed to freely evolve on its own.

As the typhoon encountered the elevated CCN in the sensitivity tests, a significant perturbation of windspeed, convective fluxes, and hydrometeor species behavior was simulated. Early during the ingestion of enhanced CCN, precipitation was reduced due to suppressed collision and coalescence, and storm winds increased in strength. Subsequently, owing to reduced fall speeds of the smaller drops, greater amounts of condensate were thrust into supercooled levels where the drops froze releasing greater amounts of latent heat of freezing. Convection thereby intensified which resulted in enhanced rainfall and more vigorous convectively-produced downdrafts. As the convection intensified in the outer rainbands the storm drifted over the developing cold-pools. The enhanced cold-pools blocked the inflow of warm, moist air into the core of the typhoon which led to a weakening of the typhoon with significantly reduced low level wind speeds. The very high amounts of pollution aerosols resulted in large amounts of condensate being thrust into the storm anvil which weakened convective downdrafts and cold-pools, yet the system did show reductions in windspeed (although weaker)

ACPD
12, 351–385, 2012

compared with the clean control run. This study suggests that ingestion of elevated amounts of CCN into a tropical cyclone (TC) can appreciably alter the intensity of the storm. This implies that intensity prediction of TCs would be improved by including indirect aerosol affects. However, the pollution aerosols have very little impact on the storm track.

1 Introduction

There is increasing evidence that aerosols acting as cloud condensation nuclei(CCN) can modulate the intensity of tropical cyclones (Zhang et al., 2007, 2009; Rosenfeld et al., 2007; Cotton et al., 2007, 2011; Khain et al, 2008, 2010; Khain and Lynn, 2010; Carrió and Cotton, 2011). The hypothesis proposed by Cotton et al. (2007) and Rosenfeld et al. (2007) is that seeding hurricanes with pollution-sized aerosols would lead to the following chain of responses that results in the eventual mitigation of the storm intensity. "In the outer rainbands, increasing CCN concentration results in reduced collision/coalescence, increased supercooled water aloft, enhanced convection (latent heat of freezing) and ultimately enhanced precipitation and low level cooling (evaporation). The increase in low level cold-pool coverage in the outer rainband region blocks the flow of energy into the storm core inhibiting the intensification of the tropical TC. However, the amount of suppression of the strength of the TC depends on the timing between the transport of CCN to the outer rainbands and the intensity and lifecycle stage of the outer rainband convection. The outer rainband convection needs to be strong in order for the transport of supercooled liquid water aloft to take place".

A key factor in this response is that a downdraft-induced cold-pool emanating from the peripheral rainbands of a TC can potentially act to cut off the inflow of warm, moist near sea-surface air which is critical in maintaining the energetics of the system (Wang, 2002; Zhang et al., 2007). Riemer et al. (2010) also finds evidence that the invigoration of convective activity in the outer rainbands leads to a reduction in TC intensity. That study focused on the role of vertical wind shear on the TC inflow layer.

ACPD
12, 351–385, 2012

In this paper, we use the Regional Atmospheric Modeling System (RAMS) to determine potential indirect effects of aerosols on TC development. There have been many studies examining the effects of aerosols on Atlantic TCs, often in the context of dust particles contained within the Saharan Air Layer(SAL)(Zhang et al., 2007, 2009), which makes it difficult to distinguish between the aerosol effects and the effects of a dry, stable air layer being entrained within a TC as a means to deintensification (Dunion and Valden, 2004). For this reason, this research will focus on TC development in the Western Pacific (WP), where pollution aerosol contributions are significant, yet changes in the large scale environment, such as associated with the SAL, are less likely.

A 2008 TC case study – Typhoon NURI – was selected for both its wealth of observational data and its inferred interaction with pollution aerosol particles emanating from the East Asian coast, as determined by both observational and aerosol model data. By running sensitivity tests with various CCN concentrations, this research should permit isolation of the indirect aerosol effects that could potentially modulate the intensity of TCs and as a result be important to their quantitative prediction. Particular attention is given to the development and modulation of cold-pool activity. This is achieved by examining simulated rainfall rates in the outer bands of the TC, buoyancy (Emanuel, 1994), perturbations in equivalent potential temperature (θ_e 19 September 2011.

2 Model description

For this study the Regional Atmospheric Modeling System (RAMS) version 4.3 was used (Cotton et al., 2003). Being quite malleable in terms of regional modeling and containing an advanced two-moment bin-emulating microphysics scheme (Feingold et al., 1998; Saleeby and Cotton 2004, 2008), the use of RAMS provides unique insight on aerosol interaction with various types of precipitation and cloud formation, including convective storms and TCs. It utilizes an Arakawa-C grid structure with the option for multiple two-way nested grids and the ability to add and subtract the nested grids within a simulation. The domain follows a rotated polar-stereographic transformation

ACPD
12, 351–385, 2012

horizontally and a terrain-following coordinate system vertically. A non-hydrostatic model, RAMS prognoses 14 variables: u, v, and, w wind components, ice-liquid water potential temperature, dry air density, total water mixing ratio and eight hydrometeor species (small cloud droplets, large cloud droplets, rain, pristine ice, snow, aggregates, graupel, and hail). The radiation is calculated according to the Harrington (1997) two-stream long/shortwave model. The model allows for a Kain-Fritsch convective parameterization (Kain, 2004) which is used on coarser grids. The boundary conditions allow for user-prescribed nudging time-scales.

The treatment and adjustment of CCN in RAMS will be the primary motivation of the sensitivity study of this research. The cloud droplet number is derived from a prognosed CCN field. The number of CCN that activate to form cloud droplets is a function of temperature, supersaturation, vertical velocity, and CCN concentration. In these simulations the chemistry of the aerosol is assumed to be ammonium sulfate and the mean particle radius invariant. The CCN field is user-prescribed and may be advected, consumed by nucleation scavenging, and/or diffused (Saleeby and Cotton, 2004).

3 Model configuration and experiment design

3.1 Grid configuration

During the first 36 h, RAMS was run with a single grid to quickly allow the model to acclimate itself to the initialization and nudging data as well as allow for the synoptic environment to set up. At 36 h, a second, finer, interactive grid of 3 km grid spacing was spawned to better represent the cloud-scale and convective elements of the storm. Also at this time, a balanced vortex routine (Montgomery et al., 2006) was implemented in the smaller grid. The addition of the algorithm facilitated the rapid generation of realistic convective fluxes that maintained the TC. Grid 1 consisted of 253 × 200 points horizontally while Grid 2 was 452 × 452 and centered at a latitude of 18.3° N and a

ACPD
12, 351–385, 2012

longitude of 130.1° E. Vertically, both grids stretched from 120 m at the surface to a maximum of 1500 m consisting of 20 levels. The model top height was about 18 km with a wave absorbing layer in the top most grids.

In order to capture the entire lifespan of the TC from cyclogenesis to landfall the second grid had to be moved to keep the TC within its domain and resolve the middle and outer rainbands of the storm, where the additional CCN is expected to cause changes in cold-pool parameters. For this reason, Grid 2 was manually-moved twice throughout the simulation. This is a similar approach to explicitly resolving convection and microphysical effects at cloud scale used by van den Heever et al. (2006) simulating convective sea-breeze forced storms. The first move occurred at 60 h from the initial time of the simulation (24 h after it was imposed). The grid was moved 375 km west and 225 km north. The second move occurred at 72 h after the simulation start (12 h after the first move) and was moved another 300 km west and 75 km further north. The location of Grid 1 and the three positions of Grid 2 are shown in Fig. 1. The entire simulation duration was 96 h, beginning on 17 August 2008, 00:00 GMT and finishing on 21 August 2008, 00:00 GMT.

Convection was parameterized on Grid 1 using a Kain-Fritsch (Kain, 2004) cumulus parameterization scheme, but explicitly resolved for the finer grids. The time step for the larger grid was 30 s and 15 s for the smaller grid.

3.2 Model initialization

The Barnes objective analysis routine (Barnes, 1973) was used for model initialization, allowing for both gridded and irregularly spaced point data. The gridded data utilized were the NCEP/NCAR Reanalysis 1 global gridded data (Kalnay et al., 1996) while the point data were assimilated from THe Observing Research and Predictability Experiment (THORPEX) Pacific Asian Regional Campaign (T-PARC) dropsondes. The internal nudging of the model occurred every 900 s during the first 36 h after which point, the internal nudging was switched off and only the boundary conditions were nudged every 450 s.

ACPD
12, 351–385, 2012

Reynolds weekly SSTs (Reynolds and Smith, 1994) were used and not updated during the simulation. The Harrington (1997) parameterization was used for long/shortwave radiation and updated every 15 m, and the Klemp and Wilhelmson (1978) boundary conditions were applied at the lateral boundaries.

3.3 Aerosol prescription

Typhoon NURI was chosen as the case study for this paper in part due to its path which took it near centers of high aerosol concentrations. As shown in Fig. 2, the AOD in and near the TC path is significantly higher than the cleaner maritime environment in which TC genesis occurred. Geography and geometry of the trend of AOD was taken into account when constructing this experiment. The MODIS retrievals show the aerosol concentration at elevated levels from the middle of China, then gently sloping in a northeasterly direction over Japan and continuing East outside of the model domain. The elevated aerosol region provided by MODIS is further confirmed by the SPRINTARS three-dimensional aerosol model (Takemura et al., 2000) data for the dates of the TC which show aerosol plumes of Sulfate and dust emanating from the Chinese and Indian coasts advecting into the path of the TC. These data guided the aerosol prescription used for this study. The CCN prescription in the simulation follows the same middle to northeastern path through the model domain and is regenerated every 6 h to represent the continual influx of aerosol from the urban centers and the Gobi desert. As a result the northwest rainbands of the simulated TC entered the regions of elevated concentrations of CCN first.

The vertical profile of CCN concentration was also constructed based on the SPRINTARS model. We use the Beijing SPRINTARS data as a guide to develop a vertical profile of CCN. The vertical CCN prescriptions for the sensitivity studies are shown in Fig. 3 and applied at each grid space within the geometric domain indicated by MODIS retrievals of elevated aerosol concentrations. In all, five simulations were conducted with varying levels of CCN concentrations within the perturbed aerosol field: 100, 400, 1000, 3000, and 5000 CCN cm^{-3}, with the 100 CCN simulation acting as the

ACPD
12, 351–385, 2012

clean background maritime control experiment. The naming conventions used for the remainder of this text identifying each simulation are listed in Table 1.

Ice nuclei and giant CCN were not varied in this experiment, and were applied three-dimensionally homogeneously at low, background concentrations. Table 2 summarizes the model configuration and options for the TC NURI simulations.

4 Results

4.1 Droplet size and precipitation

The link between extreme concentrations of CCN and droplet size is confirmed in Fig. 4. CCN were ingested into the storm at about the 58 h mark in all simulations. From that point forward, we see a marked response in cloud droplet size, particularly in the outer rainbands (50–150 km from TC center). In the most highly polluted case the mean cloud droplet diameter is smaller throughout the simulation. Being smaller, droplet collection is suppressed and riming growth of ice particles is also suppressed. As the TC drifted west, further into the elevated CCN field emanating from the Chinese coast, and the CCN became entrained in the system, the CCN made its way to the TC center. By the 72 h mark, the CCN was almost entirely wrapped around the TC, however, the southeast corner of the storm had not been fully enveloped by the enhanced CCN.

4.2 Supercooled cloud liquid water(SCLW)

The time evolution of the amount of SCLW within the outer domain of the TC is shown in Fig. 5. The low-to-high CCN concentration simulations (C400, C1000, and C3000) all show a time delay of the maxima SCLW compared to the C100 case. These simulations reach their maxima 2 h later than in the control run. The C3000 simulation shows the greatest increase in SCLW, exceeding the control simulation by 1000 kg. This is by far the greatest amplitude change, however, each simulation shows a distinct variance

ACPD
12, 351–385, 2012

in time of peak SCLW, with the most polluted case, C5000, showing the latest peak in SCLW.

4.3 Downward flux

Downward flux (DFX) is defined in (Riemer et al., 2009) as

$$\mathrm{DFX} = \theta_e' \_w, \quad (1)$$

where θ_e' is the deviation of equivalent potential temperature from the azimuthal mean and $\_w$ is the vertical velocity. This parameter yields an indication as to both the upward and downward motion and the thermodynamics of the air being transported vertically. Essentially, in a period of high convection and precipitation, the net downward flux will be strongly positive in cold-downdrafts and warm updrafts. As suggested in Riemer et al. (2009), DFX is calculated for the model height corresponding to about 1500 m to best represent the inflow from the BL. The closest model height available for this study was 1300 m, so all DFX calculations occur at that level. The time evolution of net DFX throughout the simulation is shown in Fig. 6. All simulations generally follow the same trend of DFX: each local maximum is generally located at the same model hour (t = 68, 78 h). All sensitivity tests show an initial damping of positive DFX compared to the control simulation until 68 h. At this point all simulations except C5000 quickly show an amplified DFX. The C3000 simulation shows a dramatic increase in DFX at this point in the simulation, jumping to nearly 10 000 K m s^{-1}. We also note that the C5000 case deviates little from the C100 case after the 60 h mark: the DFX minima and maxima are not as strong as in the other cases, generally staying within 2000 to 4000 K m s^{-1}.

The primary hypotheses of this study is that the entrainment of high CCN concentrations in the outer rainbands of the storm will cause an enhancement in SCLW aloft, resulting in differences in convective and cold-pool intensity in a TC. The link between SCLW and convective intensity can readily be seen in Fig. 7. Here the amount of SCLW is lag-correlated with DFX by 2 h, with the linear correlation coefficients (r) also

ACPD
12, 351–385, 2012

shown. The strong r values for the C400, C1000, and C3000 indicate a linear relationship between the presence of high SCLW and DFX 2 h later. The composite r value for all five simulations is 0.57. And if we exclude the extremely polluted case, where the vertical transport of condensate is more of a factor (discussed in detail in the next section) the correlation coefficient is 0.63: a clear sign of a positive linear correlation. The generation of large amounts of SCLW results in an eventual generation of large DFX.

We now examine the time evolution of DFX regionally compared to the TC center (Fig. 8). As we are largely concerned with the intensity of precipitation within the outer rainbands, we observe that the DFX response is stronger in the C1000 and C3000 cases when looking past 60 h and 50 to 150 km from TC center. In the C1000 simulation starting at 78 h, we see the movement of strong DFX towards the center of the TC, an artifact of the movement of the TC. A similar inward-tendency of strong DFX is evident in the C3000 simulation; however, as the additional CCN damps the DFX initially, the strongest period of DFX is stronger and closer to the TC center. The C5000 simulation shows the most neutral DFX response over the entire simulation. The maximum tangential windspeed is shown in Fig. 15, 14, exhibiting a fluctuating response akin to the DFX strength.

4.4 Cold-pool activity

For this study, we will define a cold-pool explicitly as any grid cell at or near the surface that is more than 5 K colder than the horizontal mean. With that definition in hand, we can evaluate the time evolution of the number of cold-pool grid cells throughout each simulation and determine how they differ from the control run (Fig. 9). We see in conjunction with the periods of enhanced DFX, there are periods of greater swaths of cold-pools. Similarly, for the C5000 case, which has been established to have dampened convective activity, the spatial extent of cold-pools is damped as well. For the moderately-elevated CCN cases, there is a near-uniform increase in cold-pool extent from 82 h and beyond. Hovering at around an additional 200 grid cells at 3 km × 3 km

ACPD
12, 351–385, 2012

in the nested grid, the moderately-elevated CCN cases translate to a roughly 1800 square km increase at each time step.

If we examine the equivalent potential temperature directly, we can see the aerosol impact on simulated storm dynamics. Figure 10 shows the azimuthal average around the storm of θ_e at 84 h into the simulations. In the clean, C400 case, we see a classic example of a warm-core TC with regions of high θ_e near storm-center. In the elevated CCN cases we see a suppression of the convectively-generated "hot towers" with lower θ_e air near the storm-center at or above 1500 m. Moreover, the C1000 and C3000 show a tendency for low θ_e air to dip to near-BL levels and impinge into the middle of the TC. The C5000 case, with its damped convection, shows a much more "classic" vertical and horizontal gradient of θ_e, with high θ_e near the warm-core and low θ_e elsewhere, indicating limited downdraft and convective fluxes.

4.5 Response of hydrometeors

Thus far, we have seen a monotonic increase in cold-pool activity and convective fluxes with increased CCN concentration, except for the extremely polluted case: C5000. In order to better understand the mechanisms that govern the extreme CCN case, in this section we examine the hydrometeor species individually. In this section, we will focus on five classes of hydrometeors: cloud droplets, rain droplets, pristine ice, snow, and graupel. Hail/frozen raindrops was excluded from the hydrometeor plots for clarity. Examining the aerosol impact on hydrometeors will aid in the explanation of the varying convective activity throughout the life of the TC.

Cross sections of the storm at 68 h showing the different mixing ratios for the five hydrometeors in question are plotted in Fig. 11 for C3000 and C5000. Here we see the C3000 case precipitating substantially and transitioning from ice to snow at about 10 000 m, then to graupel, then finally as cloud and rain mixing ratios below 5000 m. For the C5000 case all these five hydrometeor species are present, but with reduced mixing ratios, excepting pristine ice and cloud. The vertical distribution of ice in the C5000 case stretches well past 15 000 m while the C3000 case appears capped. Owing to

ACPD
12, 351–385, 2012

reduced collision and coalescence growth of droplets and ice particle riming, the hydrometeors in the polluted case are smaller and thereby transported to anvil levels and less likely to fall out by precipitation, sedimentation, or scavenging.

At 86 h into the simulation, and about 26 h after the storm has come in contact with the elevated aerosol levels, the C1000 and C3000 cases are very convectively active (Fig. 12). The number concentration of pristine ice stretches well above the freezing level at this point in the highly polluted cases, capping out well past 15 000 m above the surface. As at previous times, the C5000 case is vertically transporting condensate in the form of small ice particles aloft. For such small ice crystals, riming is hindered and subsequently the particles are transported to anvil levels. Wang (2005) and Carrio and Cotton (2011a) observed a similar response for large CCN concentrations in their idealized simulations of a TC. Likewise, Khain (2009), Carrio et al. (2010) and Carrio and Cotton (2011b) found a similar response in simulations of ordinary thunderstorms.

4.6 Near surface maximum windspeeds

As shown in Fig. 13, during the early period when the pollution is first ingested into the storm, near surface winds actually intensified. Later on, however, the storm weakened in strength in accordance with the basic hypothesis. As shown in Fig. 14, which illustrates the boundary of the pollution plume by the contour of the CCN concentration of 1000 cc^{-1} the pollution plume has been entirely engulfed into the storm at the time of storm weakening, The reason the storm intensified during the early period of pollution ingestion was because the pollution plume invaded the eyewall region of the storm. This resulted in delayed droplet collision and coalescence, enhanced supercooled liquid water and intensified convection in the eyewall with little interference from downdrafts and cold-pools in the nearly saturated eyewall region. Later, the pollution aerosol were prevented from reaching the storm interior due to nucleation scavenging and thereby the outer rainband convection was mainly altered leading to the weakening of the storm as in the basic hypothesis. In both the Carrio and Cotton (2011b) and these simulations the response of near-surface wind to enhanced aerosol was

ACPD
12, 351–385, 2012

monotonic up to a "tipping point" after which enhanced CCN so suppressed ice particle riming that excessive transport of water substance to anvil levels occurred. Thus the simulated maximum windspeed after the 74 h mark (Fig. 13) is reduced relative to the control for the C5000, albeit less so than the C3000 case.

4.7 Simulated storm track

The TC tracks for each experiment, along with the best track given by the Japanese National Institute of Informatics (NII) and the track of minimum geopotential height according to ECMWF model data are shown in Fig. 15. RAMS produces a storm that maintains a track error of about 1.5 degrees rather consistently throughout the simulations. The model error yielded in RAMS was similar to that of the forecasted track of the storm (Miyoshi et al., 2010). While the C5000 exhibits the highest amount of drift in the TC track, the amount it differs in track is negligible. In the dissipation phase of the storm the RAMS simulated track, the center of the TC, as indicated by minimum perturbation pressure, turns southward bringing it more in line with the NII and ECMWF indicated tracks.

5 Conclusions

The ingestion of increased CCN concentrations produced smaller cloud droplet sizes (Fig. 4), particularly in the mid to outer rainbands of the TC (50 km to 100 km from TC center) following the initial surge of pollution aerosols into the storm. Smaller liquid droplets result in three immediate effects:

1. Cloud droplet collision and coaleascence is suppressed.
2. The fall-speed of the smaller particles is reduced, causing the system to thrust more condensate to higher levels.

ACPD
12, 351–385, 2012

3. Smaller droplets are less likely to be rimed by ice particles and will be less likely to freeze at near-zero freezing temperatures. This results in elevated latent heating of freezing and therefore altering the vertical heating profile of the storm. These three immediate effects of the enhanced CCN concentrations were evident in the sensitivity tests in the form of more SCLW (Fig. 5). The increase in SCLW led to a direct increase in convectively-produced downdrafts, as shown by diagnosed DFX. Net DFX lag-correlated strongly with SCLW (Fig. 6), particularly in the moderate CCN simulations.

The increase in convective activity resulted in appreciable cold-pool modulation. As defined by raw temperature change (Fig. 9) and (Fig. 10), the cold-pool intensity differed significantly under different CCN conditions. The C3000 simulation in particular showed evidence of low θ_e air intruding into the inflow of the TC. Reimer et al. (2009) found a similar cold-pool response as vertical shear of the horizontal wind was increased rather than CCN. While it is difficult to directly attribute the cold-pool's presence, strength, and domain to TC weakening, the addition of dry, cool air acts to disrupt the energy source of a TC, as proposed by Wang (2002) and Zhang et al. (2007).

The simulated maximum low-level wind speeds increased relative to the control during the first 10 h or so after ingesting the high CCN followed by a period in which wind speeds substantially weakened and generally remained less than the control for the remainder of the simulation period. During the intensification phase, pollution aerosols covered the entire storm and convective cells throughout the TC intensified. Only later did large-area cold-pools form which contributing to a weakening of the simulated TC. The pollution aerosols have very little impact on the storm track.

This study, as all TC-aerosol studies, is by no means comprehensive. The simulations were especially regime specific, consisting of a particular CCN domain, TC intensity, meteorological background, aerosol species, etc. all of which could alter the impact of aerosols on the development of a TC. These and other variables could be explored with different regional and/or TC forecasting models in idealized simulations and/or case studies. Further cold-pool analyses could prove insightful as this study

ACPD
12, 351–385, 2012

highlighted strong cold-pool modulation of TC dynamics. In particular, observations and simulations of the mapping of cold-pools, and the TC's response to their strength, shape, size, and timing, could provide a useful indication of the subsequent behavior of a TC.

Acknowledgements. We thank Gustavo Carrio of CSU who was very helpful in setting up the numerical experiments.

This research was supported by the DoD Center for Geosciences/Atmospheric Research at Colorado State University under Cooperative Agreement W911NF-06-2-0015 with the Army Research Laboratory. Additional support was provided by the Department of Homeland Security through NOAA (NOAAESRL) contract # NA17RJ1228.

References

Carrió, G. G. and Cotton, W. R.: Investigations of aerosol impacts on hurricanes: virtual seeding flights, Atmos. Chem. Phys., 11, 2557–2567, doi:10.5194/acp-11-2557-2011, 2011.

Cotton, W. R., Pielke, R. A., Walko, R. L., Liston, G. E., Tremback, C. J., Jiang, H., McAnelly, R. L., Harrington, J. Y., Nicholls, M. E., Carrió, G. G., and McFadden, J. P.: "RAMS 2001: Current status and future directions", Meteor. Atmos. Phys., 82, 5–29, 2003.

Cotton, W. R., Zhang, H., McFarquhar, G. M., and Saleeby, S. M.: Should we consider polluting hurricanes to reduce their intensity?, J. Wea. Mod., 39, 70–73, 2007.

Cotton, W. R., Woodley, W. L., Ginis, I., Golden, J. H., Khain, A., and Rosenfeld, D.: The Rise and Fall of Hamp, J Weather Modification Association, 43, 88–95, 2011.

Dunion, J. P. and Velden, C. S.: The Impact of the Saharan Air Layer on Atlantic Tropical Cyclone Activity, B. Am. Meteorol. Soc., 85, 353–365, 2004.

Emanuel, K. A., Neelin, J. D., and Bretherton, C. S.: On large-scale circulations in convecting atmospheres, Q. J. Roy. Meteorol. Soc., 120, 1111–1143, doi:10.1002/qj.49712051902, 1994.

Feingold, G., Walko, R. L., Stevens, B., and Cotton, W. R.: Simulations of marine stratocumulus using a new microphysical parameterization scheme, Atmos. Res., 47–48, 505–528. doi:10.1016/S0169-8095(98)00058-1, 1998.

Harrington, J. Y.: The effects of radiative and microphysical processes on simulated warm and

ACPD

12, 351–385, 2012

transition season Arctic, During the completion of this stratus, Dept. of Atmospheric Science Bluebook 637, Colorado State University, Fort Collins, CO, USA, 289, 1997.
van den Heever, S. C., and Cotton, W. R.: Urban Aerosol Impacts on Downwind Convective Storms, J. App. Meteorol. Climatol., 46, 828–850, doi:10.1175/JAM2492.1, 2007.
Hendricks, E. A., Montgomery, M. T., and Davis, C. A.: The Role of "Vortical" Hot Towers in the Formation of Tropical Cyclone Diana (1984), J. Atmos. Sci., 61, 1209–1232, 2004.
Kain, J. S.: The Kain-Fritsch Convective Parameterization: An Update, J. App. Meteorol., 43, 170–181, doi:10.1175/1520-0450(2004)043<0170:TKCPAU>2.0.CO;2, 2004.
Kalnay, E., Kanamitsu, M., Kistler, R., Collins, W., Deaven, D., Gandin, L., Iredell, M., Saha, S., White, G., Woollen, J., Zhu, Y., Chelliah, M., Ebisuzaki, W., Higgins, W., Janowiak, J., Mo, K. C., Ropelewski, C., Wang, J., Leetmaa, A., Reynolds, R., Jenne, R., and Joseph, D.: The NCEP/NCAR 40-Year Reanalysis Project, Bull. Am. Meteorol. Soc., 77, 437–471, 1996.
Khain, A. P.: Effects of aerosols on precipitation: a review, Environ. Res. Lett., 4, 015004, doi:10.1088/1748-9326/4/1/015004, 2009.
Khain A. P. and Lynn, B.: Simulation of tropical cyclones using spectral bin microphysics, Hurricane research, Chapter 26, InTech Open Access Publisher, 2010.
Khain, A. P., Cohen, N., Lynn, B., and Pokrovsky, A.: Possible aerosol effects on lightning activity and structure of hurricanes, J. Atmos. Sci., 65, 3652–3667, 2008.
Khain, A. P., Lynn, B., and Dudhia, J.: Aerosol effects on intensity of landfalling hurricanes as seen from simulations with WRF model with spectral bin microphysics, J. Atmos. Sci., 67, 365–384, 2010.
Klemp, J. B. and R. B. Wilhelmson.: The Simulation of Three-Dimensional Convective Storm Dynamics, J. Atmos. Sci., 35, 1070–1096, 1978.
Montgomery, M. T. and Enagonio, J.: Tropical Cyclogenesis via Convectively Forced Vortex Rossby Waves in a Three-Dimensional Quasigeostrophic Model, J. Atmos. Sci., 55, 3176–3207, 1998.
Montgomery, M. T., Nicholls, M. E., Cram, T. A., and Saunders, A. B.: A Vortical Hot Tower Route to Tropical Cyclogenesis, J. Atmos. Sci., 63, 355–386, doi:10.1175/JAS3604.1, 2006.
Reynolds, R. W. and Smith., T. M.: Improved Global Sea Surface Temperature Analyses Using Optimum Interpolation, J. Clima., 7, 929–948, 1994.
Riemer, M., Montgomery, M. T., and Nicholls, M. E.: A new paradigm for intensity modification of tropical cyclones: thermodynamic impact of vertical wind shear on the inflow layer, Atmos. Chem. Phys. Discuss., 9, 10711–10775, doi:10.5194/acpd-9-10711-2009, 2009.

ACPD
12, 351–385, 2012

Rosenfeld, D., Khain, A., Lynn, B., and Woodley, W. L.: Simulation of hurricane response to suppression of warm rain by sub-micron aerosols, Atmos. Chem. Phys., 7, 3411–3424, doi:10.5194/acp-7-3411-2007, 2007.

Saleeby, S. M. and Cotton, W. R.: A Large-Droplet Mode and Prognostic Number Concentration of Cloud Droplets in the Colorado State University Regional Atmospheric Modeling System (RAMS), Part I: Module Descriptions and Supercell Test Simulations, J. Appl. Meteorol., 43, 182–195. doi:10.1175/1520-0450(2004)043<0182:ALMAPN>2.0.CO;2, 2004.

Saleeby, S. M. and Cotton, W. R.: A binned approach to cloud droplet riming implemented in a bulk microphysics model, J. Appl. Meteorol. Clim., 47, 694–703, 2008.

Seifert, A. and Beheng, K. D.: A two-moment cloud microphysics parameterization for mixed-phase clouds, Part 1: Model description, Meteorol. Atmos. Phys., 92, 45–66, doi:10.1007/s00703-005-0112-4, 2005.

Storer, R. L., van den Heever, S. C., and Stephens, G. L.: odeling Aerosol Impacts on Convective Storms in different enviroments, J. Atmos. Sci., 9, 100903135953021, 3904–3915 , doi:10.1175/2010JAS3363.1, 2010.

Takemura, T., Okamoto, H., Maruyama, Y., Numaguti, A., Higurashi, A., and Nakajima, T.: Global three-dimensional simulation of aerosol optical thickness distribution of various origins, J. Geophys. Res., 105, 17853–17873, 2000.

Tompkins, A. M.: Organization of Tropical Convection in Low Vertical Wind Shears: The Role of Cold Pools, J. Atmos. Sci., 58, 1650–1672, 2001.

Wang, C.: A modeling study of the response of tropical deep convection to the increase of cloud condensational nuclei concentration: 1. Dynamics and microphysics, J. Geophys. Res., 110, D21211, doi:10.1029/2004JD005720, 2005.

Wang, Y.: An Explicit Simulation of Tropical Cyclones with a Triply Nested Movable Mesh Primitive Equation Model: TCM3, Part II: Model Refinements and Sensitivity to Cloud Microphysics Parameterization*, Mon. Weather Rev., 130, 3022–3036, 2002.

Wang, Y.: How Do Outer Spiral Rainbands Affect Tropical Cyclone Structure and Intensity?*, J. Atmos. Sci., 66, 1250–1273, doi:10.1175/2008JAS2737.1, 2009.

Zhang, H., McFarquhar, G. M., Saleeby,S. M., and Cotton, W. R.: Impacts of Saharan dust as CCN on the evolution of an idealized tropical cyclone, Geophys. Res. Lett., 34, L14812, doi:200710.1029/2007GL029876, 2007.

ACPD
12, 351–385, 2012

Zhang, H., McFarquhar, G. M., Cotton, W. R., and Deng, Y.: Direct and indirect impacts of Saharan dust acting as cloud condensation nuclei on tropical cyclone eyewall development, Geophys. Res. Lett., 36, L06802, doi:200910.1029/2009GL037276, 2009.

ACPD
12, 351–385, 2012

Table 1. Naming conventions used for this study of each sensitivity test simulation of TC NURI as well as the control run.

Simulation Identifier	CCN concentration of elevated aerosol field (m^{-3})
C100 or "Control"	100
C400 or "Moderately clean"	400
C1000 or "Moderately polluted"	1000
C3000 or "High"	3000
C5000 or "Extreme"	5000

ACPD
12, 351–385, 2012

Table 2. RAMS model configuration and options. Azimuthal average of DFX by time for each sensitivity test plotted with the maximum tangential windspeed.

Model Aspect	Setting
Grid	Arakawa C grid Two grids Grid 1: $\Delta x = \Delta y = 15$ km; 253 × 200 Grid 2: $\Delta x = \Delta y = 5$ km; 452 × 452 Manual moving of Grid 2, follows TC path Vertical grid: Δz stretchesfrom 120 m to 1500 m; 20 vertical levels
Initialization	Barnes objective analysis NCAR/NCEP Reanalysis Data T-PARC Dropsondes
Time Step	Grid 1: 30 s; Grid 2: 15 s
Simulation duration	96 h 08/17/2008 to 08/21/2008
Microphysics scheme	Two-moment bin emulating microphysics (Meyers et al., 1997; Feingold et al.,1998;)
Convective initiation	Kain-Fritsch parameterization (Kain, 2004) for Grid 1; explicit convection on Grid 2
Radiation scheme	Harrington, (1997)
Sea Surface Temperatures	Reynolds weekly SSTs (Reynolds and Smith, 1994)
Aerosol Prescription	Horizontal domain based on MODIS AOD retrievals and SPRINTARS model output Vertical CCN profile of sensitivity tests based on SPRINTARS (Fig. 6) Regenerated every 6 h

ACPD
12, 351–385, 2012

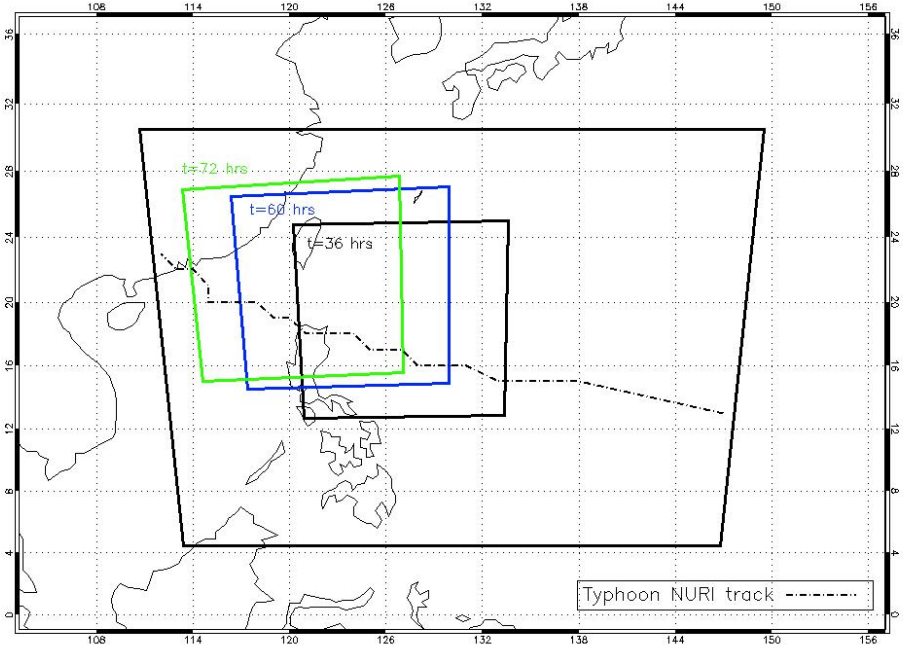

Fig. 1. A map showing the location of Grid 1 and the three locations of the manually moved finer Grid 2. The track of TC NURI according to the Japanese National Institute of Informatics (NII) is shown for clarity.

ACPD
12, 351–385, 2012

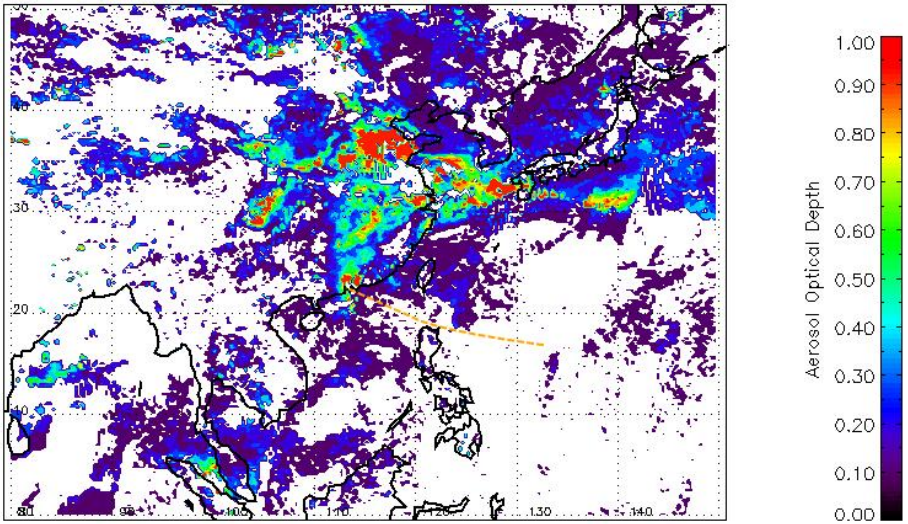

Fig. 2. The AOD retrieved from MODIS averaged over the lifespan of TC NURI (path shown as dashed orange line).

ACPD
12, 351–385, 2012

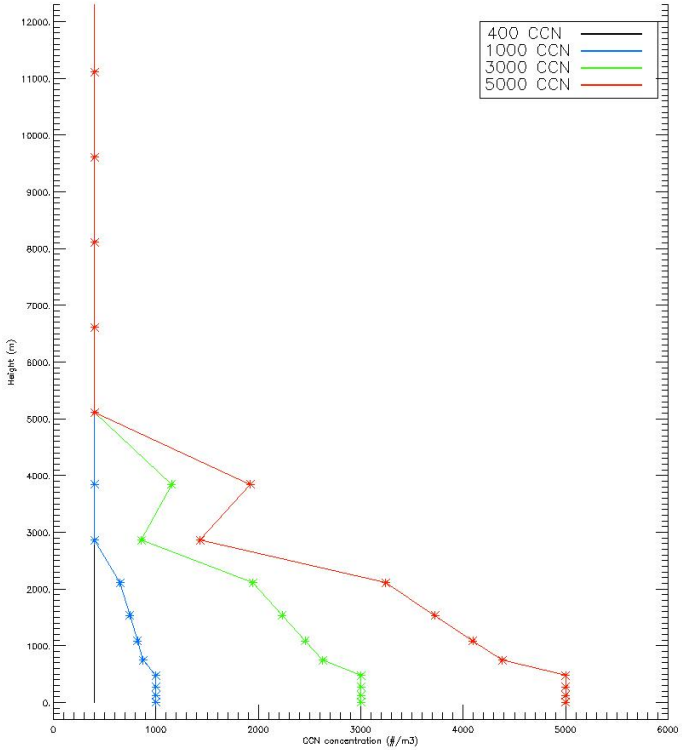

Fig. 3. The prescribed vertical CCN profile for the four sensitivity experiments conducted.

ACPD
12, 351–385, 2012

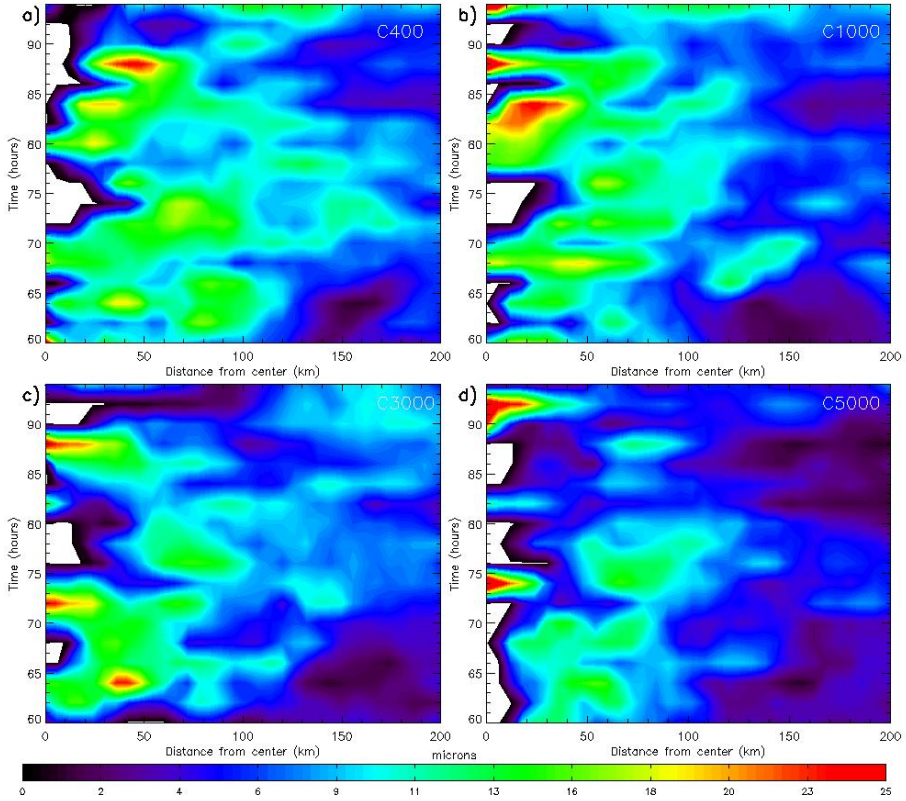

Fig. 4. Azimuthally averaged cloud droplet diameter (microns) according to distance from TC center by time for all sensitivity tests **(a)** C400; **(b)** C1000; **(c)** C3000; **(d)** C5000).

ACPD
12, 351–385, 2012

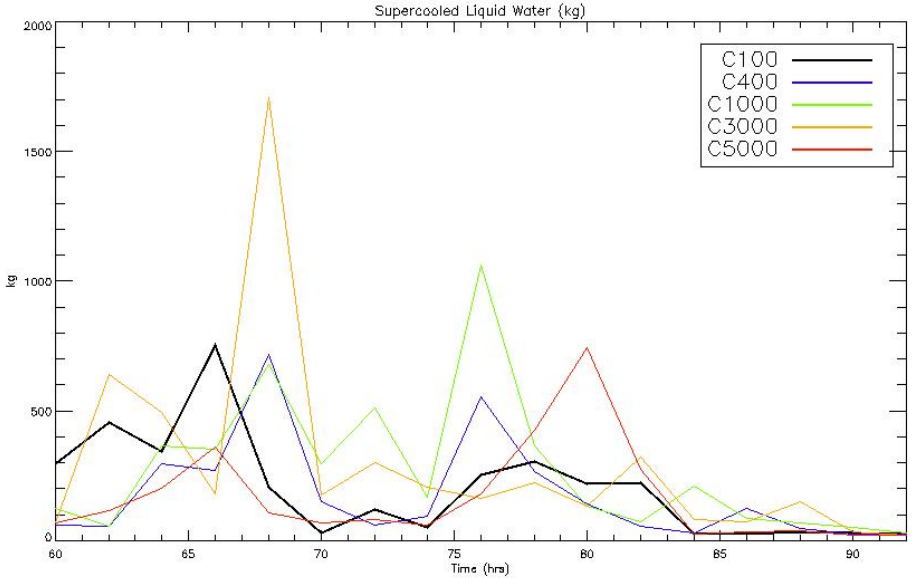

Fig. 5. The total amount of SCLW (kg) within the 250 km of TC center by time for each simulation.

ACPD
12, 351–385, 2012

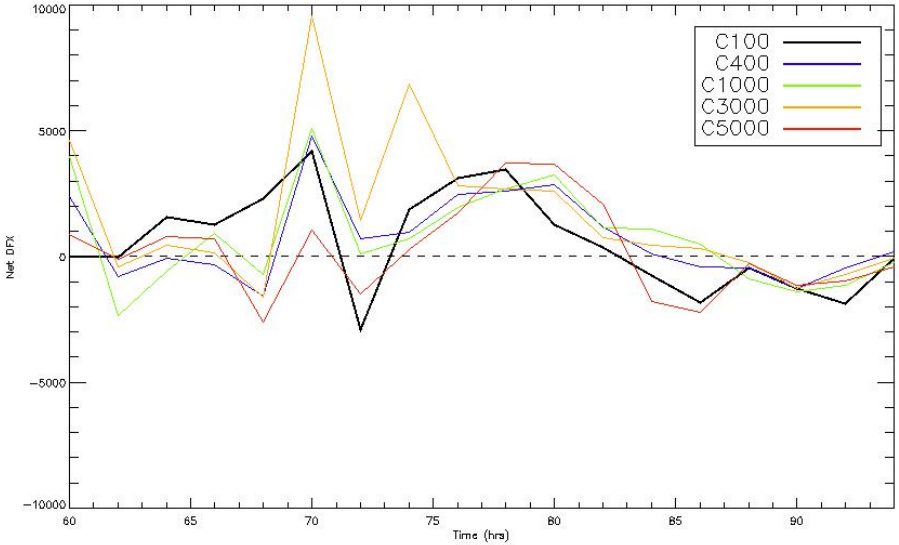

Fig. 6. Net DFX over the inner grid domain at 200m height at over the course of each simulation for control simulation and all sensitivity tests.

ACPD
12, 351–385, 2012

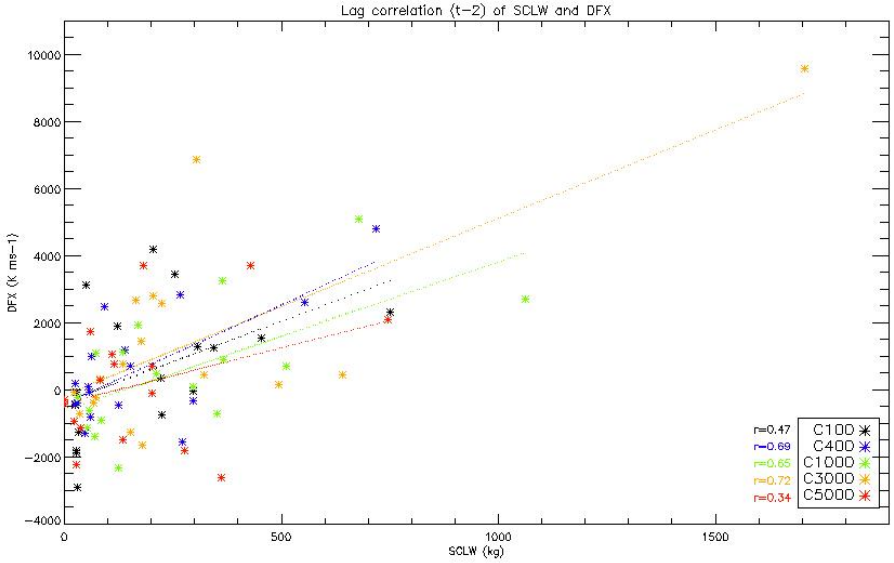

Fig. 7. Scatterplot of SCLW and DFX lagged two hours for all simulations. Linear correlation coefficients (r) for each simulation are shown. The composite r value is 0.57.

ACPD
12, 351–385, 2012

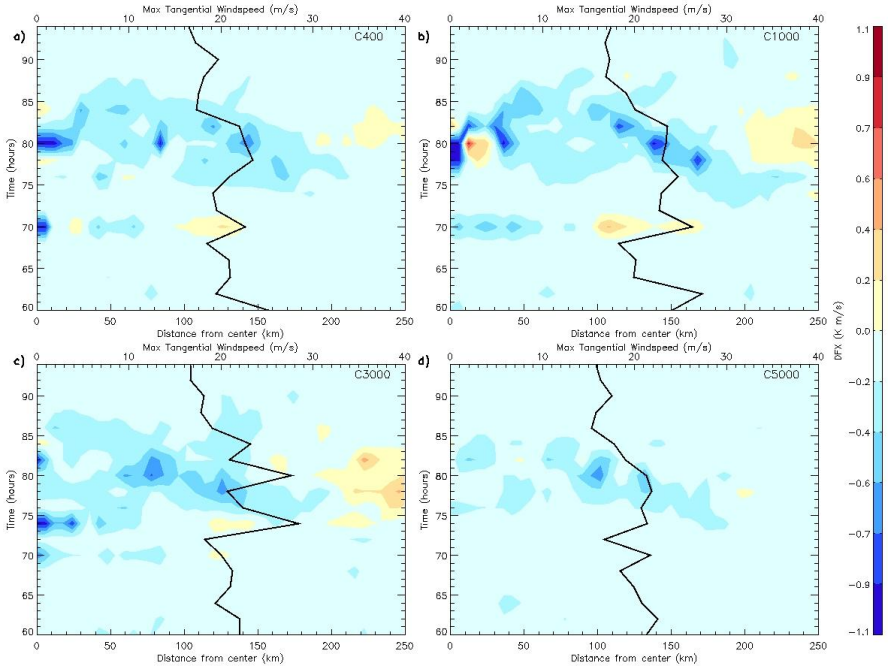

Fig. 8. Azimuthal average of DFX by time for each sensitivity test plotted with the maximum tangential windspeed.

ACPD
12, 351–385, 2012

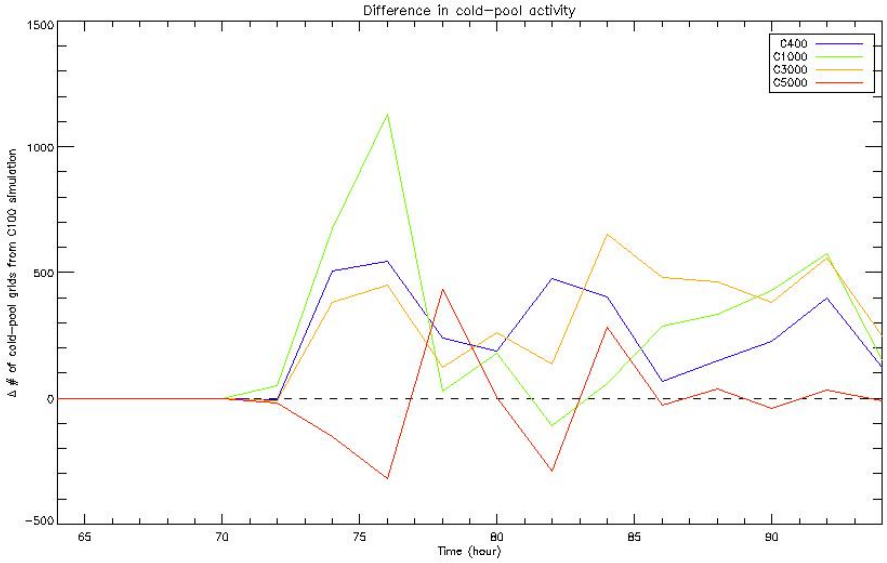

Fig. 9. Change in the number of cold-pool grid cells (see text for definition) for nested grid from C100 simulation over time.

ACPD
12, 351–385, 2012

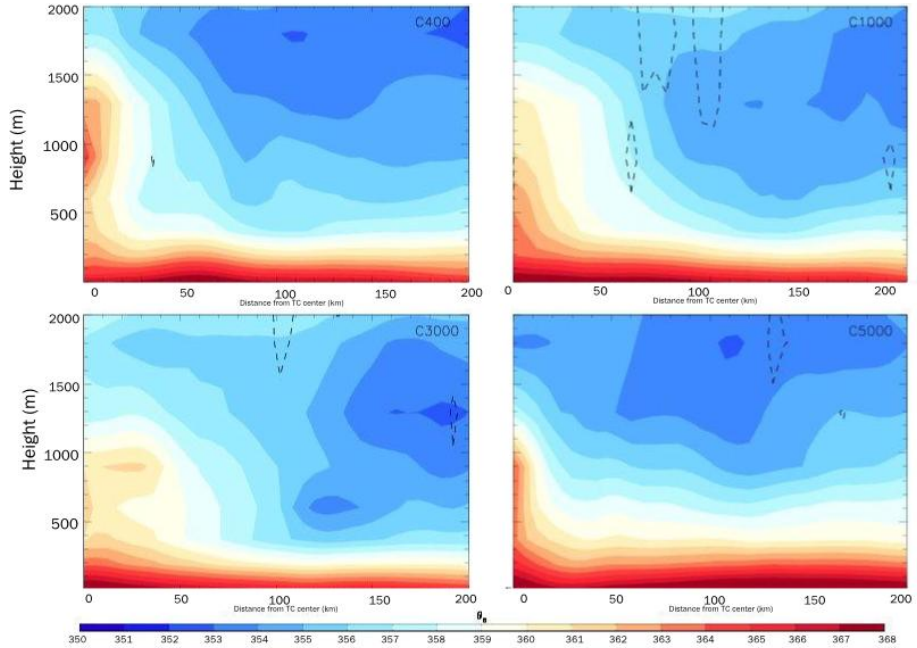

Fig. 10. Azimuthal average of according to height at $t = 84$ h. Azimuthal average of downdraft contours of $-0.5\,\mathrm{m\,s^{-1}}$ are also plotted (dashed lines).

ACPD
12, 351–385, 2012

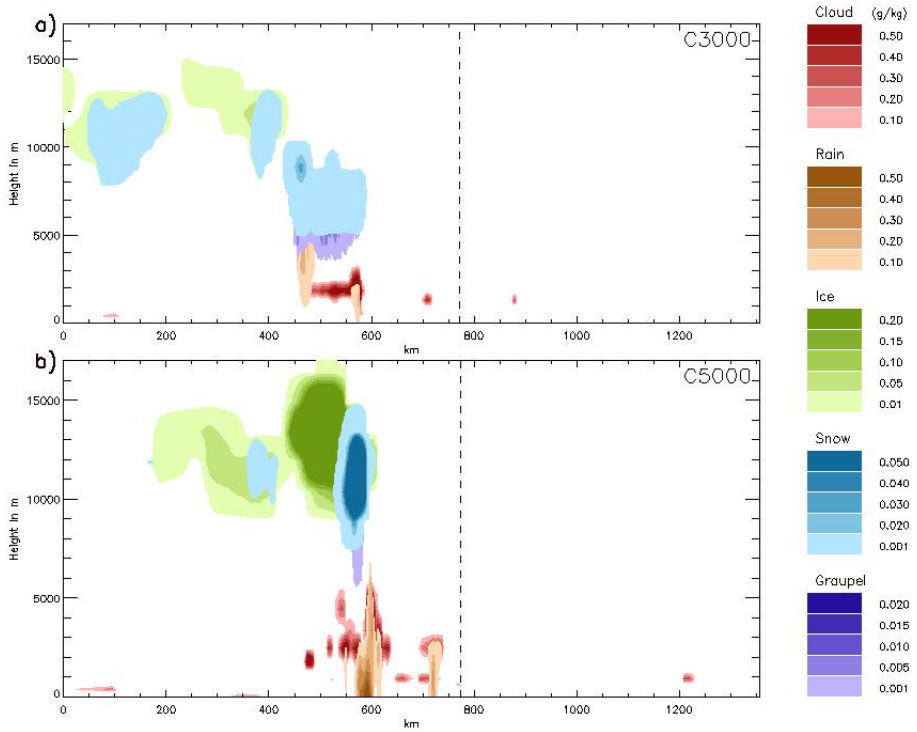

Fig. 11. Cross section of storm at $t = 68$ h showing mixing ratios for five selected hydrometeor species for C3000 **(a)** and C5000 **(b)** cases. Center of TC according to minimum sea level pressure is also plotted (dashed line).

ACPD
12, 351–385, 2012

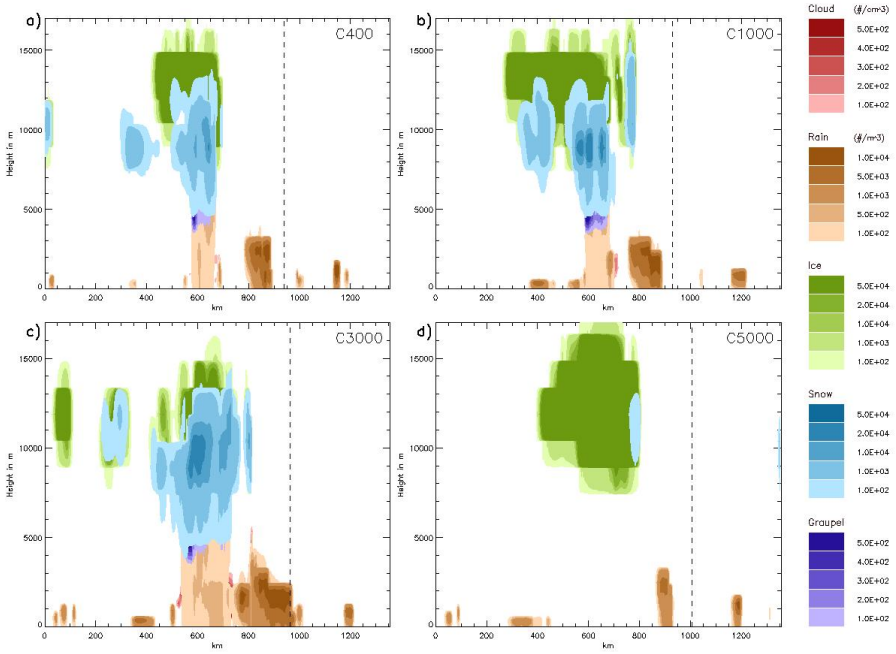

Fig. 12. As Fig. 10, but for number concentration and all sensitivity tests at $t = 86$ h.

ACPD
12, 351–385, 2012

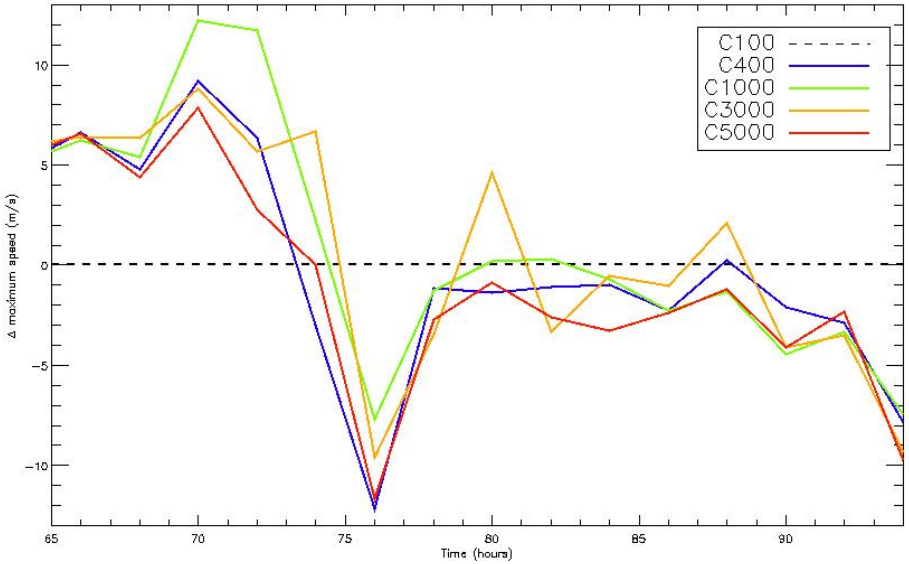

Fig. 13. Difference of near surface maximum windspeeds from the C100 case for each sensitivity tests.

ACPD
12, 351–385, 2012

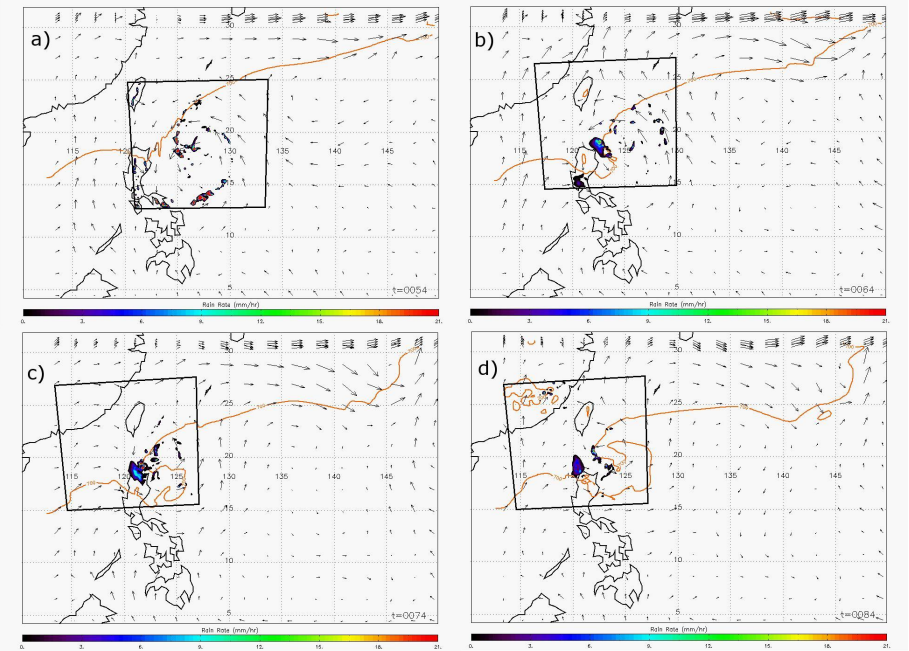

Fig. 14. : The track of TC from each sensitivity test as determined by perturbation pressure and NII best track and ECMWF Reanalysis Data as given by geopotential height.

ACPD
12, 351–385, 2012

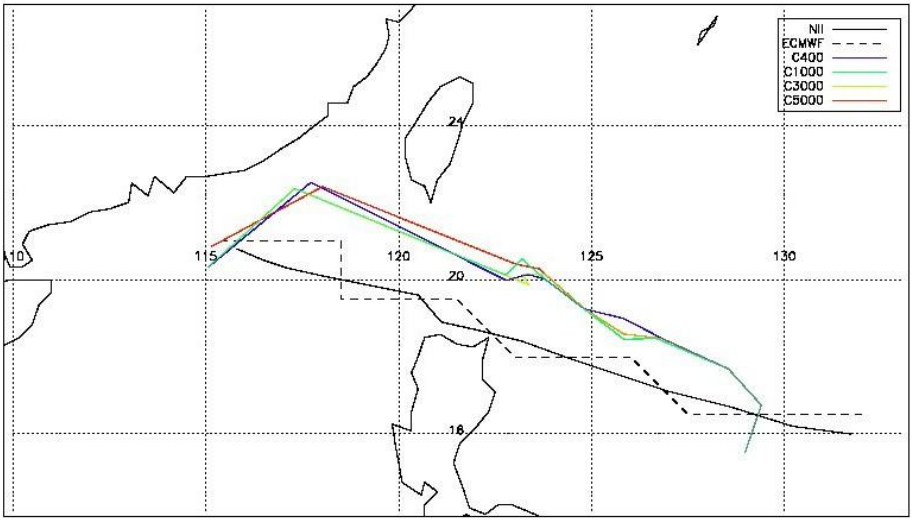

Fig. 15. The track of TC from each sensitivity test as determined by perturbation pressure and NII best track and ECMWF Reanalysis Data as given by geopotential height.

ACPD
12, 351–385, 2012